SCIENTIFIC REPORTS

OPEN

Non-synchronization of lattice and carrier temperatures in light-emitting diodes

Received: 26 August 2015
Accepted: 14 December 2015
Published: 20 January 2016

Jihong Zhang[1], Tienmo Shih[2,3], Yijun Lu[1], Holger Merlitz[2,4], Richard Ru-Gin Chang[5] & Zhong Chen[1]

Pulse implementation or switching-off (PISO) of electrical currents has become a common operation in junction-temperature (T_j) measurements for semiconductor devices since 2004. Here we have experimentally discovered a substantial discrepancy between T_j values with, and without, PISO (e.g., 36.8 °C versus 76.5 °C above the ambient temperature at 25.0 °C). Our research indicates that methods associated with PISO are flawed due to non-synchronization of lattice temperatures and carrier temperatures in transient states. To scrutinize this discrepancy, we propose a lattice-inertia thermal anchoring mechanism that (1) explains the cause of this discrepancy, (2) helps to develop a remedy to eliminate this discrepancy by identifying three transient phases, (3) has been applied to establishing an original, accurate, and noninvasive technique for light-emitting diodes to measure T_j in the absence of PISO. Our finding may pave the foundation for LED communities to further establish reliable junction-temperature measurements based on the identified mechanism.

In designing light-emitting diodes (LEDs)[1–3] that emit the light via recombination of holes and electrons and waste thermal energy through lattice vibration, we desire to extract photons (P_{opt}), must supply electrons (P_{elec}), and dislike phonons (P_{cond}) (Fig. 1a). In turn, characteristics of photons, electrons, and phonons are strongly associated with the temperature at the junction interface (T_j) between n-type and p-type semiconductors[4–7]. It is currently a challenge to accurately measure LED junction temperatures[8–11] (T_j) under conditions of large currents[12–15]. The primary reason arises because LED chips are usually sealed, thus prohibiting direct contacts. Presently, the work related to pulse implementation or switching-off (PISO, Fig. 1b) has populated the literature in semiconductor areas, including forward voltages[16,17], peak energy[18,19], reverse currents[20], and low forward currents[21]. Although these methods are capable of facing the challenge mentioned above, the discrepancy between results obtained with, and without, PISO has been found to be substantial.

In our laboratory, we have adopted both the forward voltage method (FVM, Fig. 1b) and confocal Raman spectroscopy (CRS, Fig. 1c). Using the former, we first obtain the steady-state linear relationship between T_j (inset of Fig. 2a), controlled by the heat sink at $T_{sink} = 25.0$ °C, and the forward voltage V at 5 mA with negligible thermal power input. Then we light the LED sample (e. g. blue InGaN/GaN) under a large steady-state current (e. g. $I_\alpha = 350$ mA). Instantaneously, this current is switched down to $I_\beta = 5$ mA by the FVM instrument named T3ster (MicRed. Inc., Hungary), and the forward voltage is recorded. Utilizing the linear relationship at 5 mA, we deduce the desired T_j to be 36.8 °C under 350 mA (Fig. 2a, time in logarithmic scale). Alternatively, when using CRS[22–24], which excludes PISO, we obtain T_j to be 76.5 °C based on the peak location of Raman shift (Fig. 2b,c). Peaks of Raman-light-beam intensity shift to the left as T_j increases by an increment of 10.0 °C, whereas the peak at $I = 350$ mA and $T_{sink} = 25.0$ °C (the ▲ curve) is located at 568.4 cm^{-1} (Fig. 2d). This trend clearly suggests that T_j must be at least higher than approximately 55.0 °C + 10.0 °C. Had T_j been lower than 55.0 °C, as measured by FVM, the peak should have been located between 569.0 cm^{-1} and 569.4 cm^{-1}. Relative to the ambient temperature at 25.0 °C, the discrepancy amounts to (51.5 °C − 11.8 °C) / 11.8 °C = 336.4%.

[1]Department of Electronic Science, Fujian Engineering Research Center for Solid-state Lighting, State Key Laboratory for Physical Chemistry of Solid Surfaces, Xiamen University, Xiamen 361005, China. [2]Department of Physics, Xiamen University, Xiamen 361005, China. [3]Institute for Complex Adaptive Matter, University of California, Davis, CA 95616 USA. [4]Leibniz Institute for Polymer Research, Dresden, Germany. [5]Shineraytek Optoelectronics Co., Shanghai 201300, China. Correspondence and requests for materials should be addressed to T.S. (email: tmshih@xmu.edu.cn) or Z.C. (email: chenz@xmu.edu.cn)

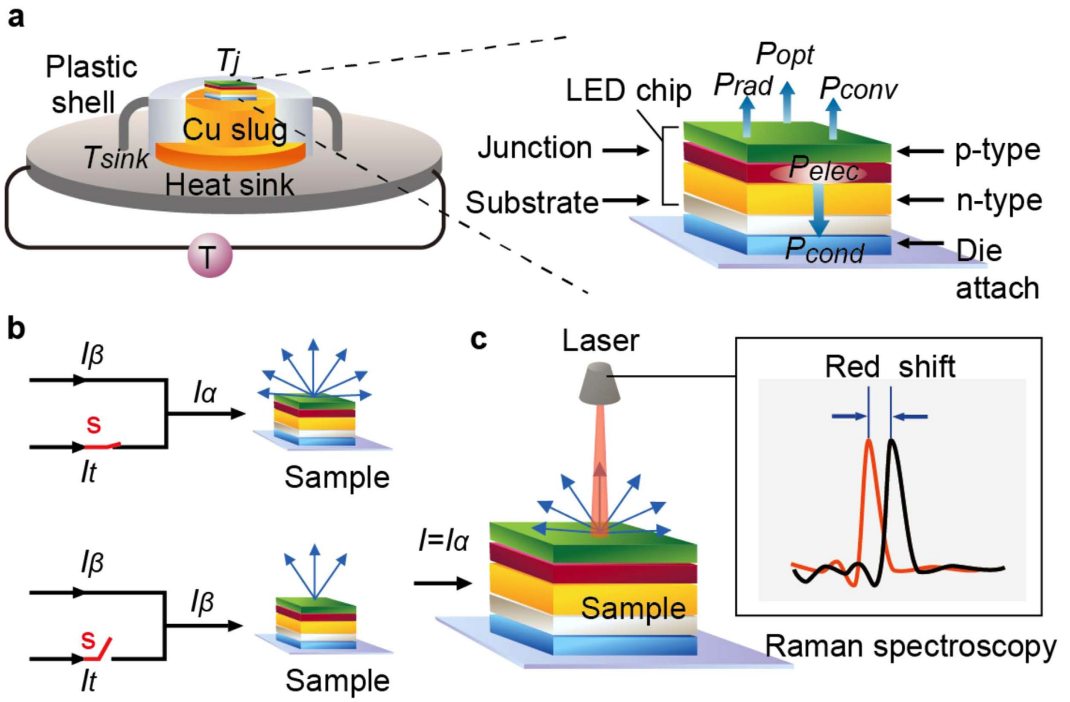

Figure 1. Experimental set-ups for forward voltage method (FVM). (**a**) The LED sample consists of layers including LED chip, die attach, and copper slug. In steady state, the influx IV should equal out fluxes including P_{cond}, P_{opt}, P_{conv}, and P_{rad} (cond = conduction; opt = optical; conv = convection; rad = radiation). (**b**) Pulse-implementation or switching-off (PISO) of currents for FVM. I_α = current at the steady state, e. g., 350 mA; I_β = a small fraction of I_α to stay on, e. g., 5 mA; I_t = the major portion of I_α to be switched off. The subscript '*t*' denotes 'thermal', suggesting that the current generates the thermal power. (**c**) Confocal Raman spectroscopy (CRS). The LED sample is mounted on a heat sink, and is lit by a current source. The peak of Raman shift has moved leftward minutely when temperatures of samples increase.

To scrutinize this puzzling difference, we have additionally used thermocouples (TC)[25] and a thermal imager (TI)[26], which receive direct thermal signals from samples, and have obtained 73.5 °C and 73.8 °C (Fig. 2e–g), respectively (Supplementary S1). Nine exposed LEDs (1-W each) were further selected for conformations, including three blue InGaN/GaN (B1#, B2#, B3#), three green InGaN/GaN (G1#,G2#, G3#) and three red AlGaInP (R1#, R2#, R3#), also leading to substantial discrepancies (Supplementary S2). Finally, we propose the following mechanism to explain this discrepancy, and further develop an independent method that requires neither PISO nor intrusive contacts, and utilizes Shockley equation for diodes as well as the principle of thermal anchoring (to be described below).

Lattice-inertia thermal anchoring (LITA)

Consider the electron transport inside a doped semiconductor undergoing three transient phases: (1) PISO phase from state α to state β, (2) non-synchronization phase from state β to state β' (a delayed state replacing state β), (3) relaxation phase from state β' to γ (steady state). The electron velocity at steady state α should equal the vector sum of the thermally-diffusive velocity and the drift velocity. After algebra, we can prove that the kinetic energy of electrons at state α is greater than the counterpart at state β ($v_\alpha^2 > v_\beta^2$) (Supplementary S3), partly because the drift component diminishes upon PISO. Electrons with small drift velocities descend to combine with holes in the valence band, reducing potential energies relative to their nucleuses. Consequently, the carrier temperature (T_c)[27–31] decreases from state α to state β. Next, there exist two types of external inputs, electrical power and thermal power that influence both T_j and T_c (Fig. 3a). For the former which drives the electron transport, I and V change instantaneously after PISO, exerting impacts on the electrical field, which subsequently causes reductions of T_c or carrier potential energy. Because of lattice inertia $\gg$ carrier inertia and the occurrence of PISO, we can conclude that $T_{c\alpha} - T_{c\beta} \gg T_{j\alpha} - T_{j\beta} \approx 0$. Consider a practical example, in which the electrical current of 350 mA (I_α) is instantaneously switched down to 5 mA (I_β) within approximately 1 μs, along with a voltage reduction from $V_\alpha =$ 3.1 V to $V_\beta =$ 2.6 V (Fig. 3b). Complicated phenomena, including re-thermalization, radiative recombination, non-radiative Auger, and non-radiative Shockley-Reed-Hall deep-level recombinations, diminish as time elapses within the sample. Let us calculate dimensionless percentage changes of V, I, and T as $|(V_\beta - V_\alpha)/V_\beta| = 0.2, |(I_\beta - I_\alpha)/I_\beta| = 69.0, |(T_{j\beta} - T_{j\alpha})/T_{j\beta}| \approx 0$, and $|(T_{c\beta} - T_{c\alpha})/T_{c\beta}| \approx |(V_\beta I_\beta - V_\alpha I_\alpha)/V_\beta I_\beta| = 84.6$. These changes imply that ΔT_j and ΔT_c differ substantially, leading to the chaotic nature of state β and the difficulty of determining $T_{c\beta}$ and V_β accurately. Hence, if possible, we should avoid utilizing data that belong to the uncertain β state, completely dismiss V_β that plays the primary role of the discrepancy-inducing

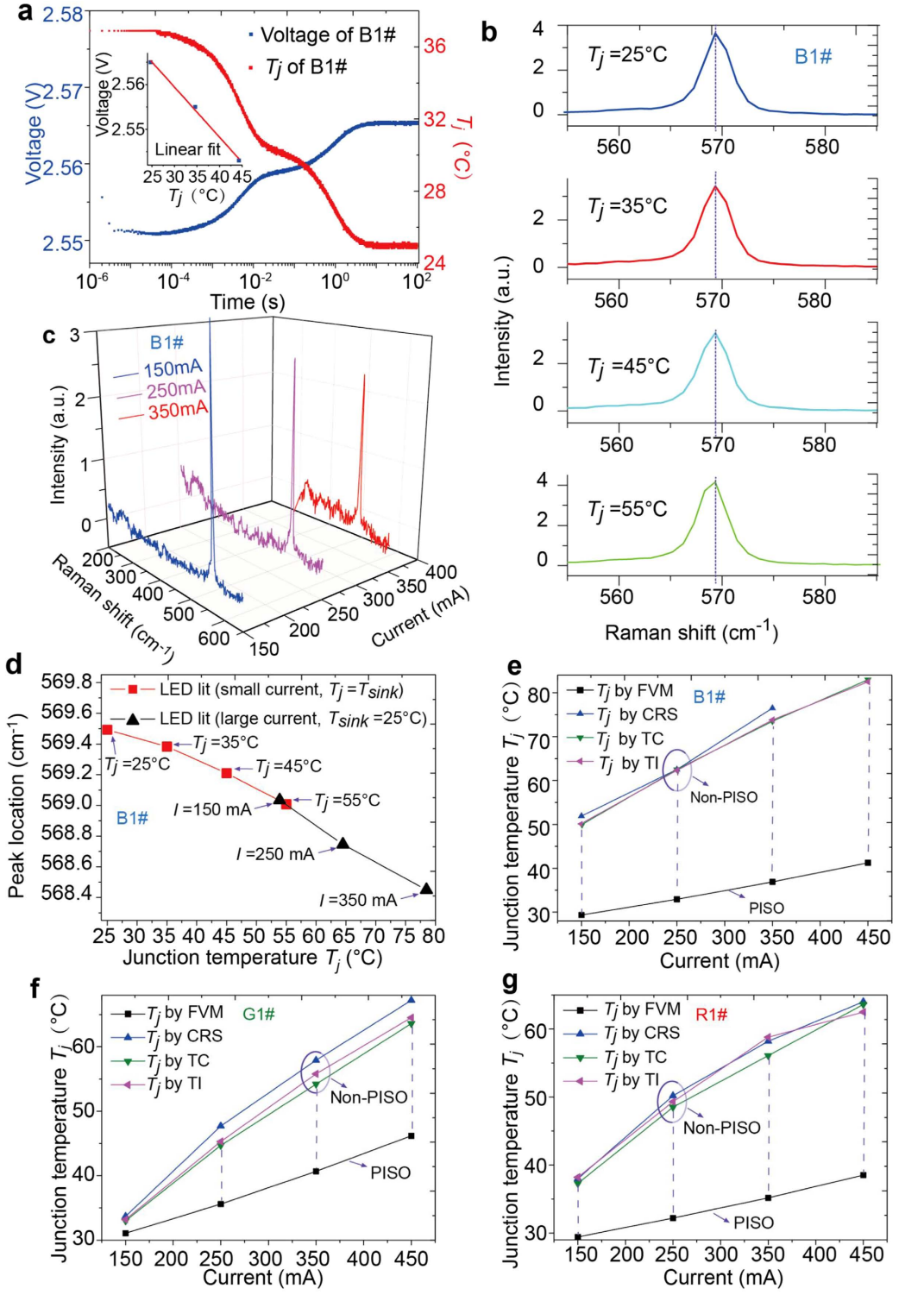

Figure 2. Junction-temperature measurements of FVM, CRS, TC and TI. (**a**) Take blue InGaN/GaN LED (B1#) as the example. In reference to the linear relationship between V and T_j, we deduce the value of $T_{j\alpha}$ to be 36.8 °C. (**b**) Relationship between T_j and Raman redshift for the B1# sample when the LED chip is lit at small currents (5 mA). The peak at $T_j = 55.0$ °C has shifted to the left slightly. (**c**) Relationship between T_j and Raman redshift for B1# sample when the LED chip is lit at large currents. At steady state and $I = 350$ mA, for example, we measure Raman shift to obtain the peak location. Next, utilizing the T_j and Raman shift relationship in **b**, we obtain $T_j = 76.5$ °C. (**d**) Correlation between peak location and T_j. (**e**) Junction temperature versus the current for B1# sample. In the absence of PISO, results obtained by CRS, TC and TI agree closely with one another, but differ appreciably from those obtained by FVM. Due to the disturbance of large noises, T_j cannot be reliably measured in CRS for B1# sample at 450mA. (**f**) Junction temperature versus the current for G1# sample. (**g**) Junction temperature versus the current for R1# sample.

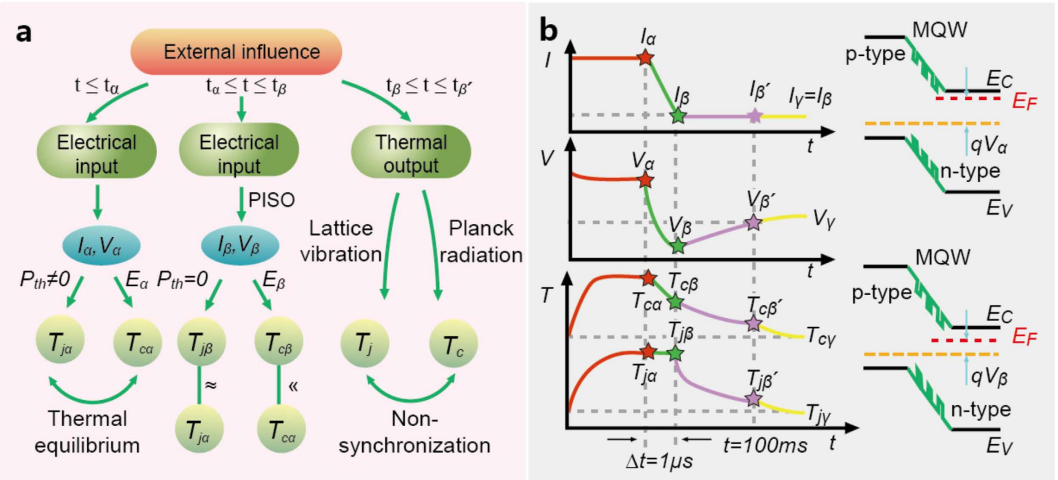

Figure 3. Microscopic system schematic explaining lattice-inertia thermal anchoring (LITA). (**a**) Non-synchronization between T_j and T_c from state α to state β'. (**b**) Time evolutions of I, V, and T at various states: α, β, β', and γ. For $t < t_\alpha$, I_α equals $I_\beta + I_t$. At $t = t_\alpha$, the switch for I_t is suddenly turned off (PISO). For $t < t_\alpha$, V_α indicates the difference between E_F in the absence and the presence of external voltage. At $t > t_\alpha$, because the current has been switched down, V_α is reduced to V_β. All samples contain multiple-quantum wells (MQW) to elevate illuminating efficiencies, as shown.

culprit, and proceed to cool down the sample further till state β'. From state β to state β', T_j is primarily influenced by the external cooling macroscopically or phonon propagation and lattice vibrations microscopically (Fig. 3a). By contrast, electrons continue to descend from higher to lower energy levels, but the descending distance becomes smaller than that from state α to state β. This loss in kinetic and potential energies is converted into the outgoing Planck radiation at larger wavelengths. Even though the magnitude of Planck radiation appears small, it is the primary macroscopic thermal cooling mechanism for T_c. According to the principle of energy conservation over a control volume containing carriers only, we obtain

$$m_c c_{v,\,c} dT_c/dt = \xi\left(V(t)I_\gamma + \sigma T_\infty^4\right) - \sum_{i=1}^{n_i} N_i h\nu_i\left(T_c,\, T_j\right), \tag{1}$$

where m_c is the effective mass of carriers, ξ the percentage of external inputs that are converted into the kinetic energy of carriers, N_i the number of electrons emitting at the frequency of ν_i and n_i the number of energy states. Likewise, the lattice also proceeds to cool down due to slower oscillations of the heat-sink lattice. Based on the principle of energy conservation over the control volume containing the lattice only, we also obtain

$$m_l c_{v,\,l} dT_j/dt = (1-\xi)\left(V(t)I_\gamma + \sigma T_\infty^4\right) - \kappa_d\left(T_j - T_{sink}\right)/d, \tag{2}$$

where κ_d is the overall thermal conductivity of layers, d the thickness of layers and the subscript 'l' denotes 'lattice'. Equations (1) and (2) suggest that T_c and T_j are governed by different thermal-cooling mechanisms as well as by their appreciably-different thermal inertias ($m_c c_{v,\,c}$ and $m_l c_{v,\,l}$), dictating that they must vary at different paces. At steady states, the inter-relationship among T_j, T_c and the voltage (V) must be unique at fixed currents and sink temperatures. Therefore, it is nonrigorous for FVM to apply this inter-relationship to situations when T_j and T_c vary at different paces. In short, for given LED types and constant small ($1 \sim 10$ mA for 1-W high power LEDs) currents, FVM asserts that, even in transient states, V is a linear function of T_j only. In the proposed study, $T_c \rightarrow$ kinetic energy of carriers $\rightarrow$ different thermal-equilibrium states $\rightarrow$ Fermi levels $\rightarrow$ external voltages, where "$\rightarrow$" denotes "influences". Clearly, V is additionally affected by T_c, which varies independently (different thermal inertiasand paces) of T_j in transient states. During transient states, the small magnitude of outgoing Planck radiation reduces T_c drastically. In turn, the decrease of T_c affects V_β in an unknown sophisticated manner. At state β', changes of T_c and T_j become synchronized again, as they did at state α. In other words, in the remedial approach ($\alpha \rightarrow \beta'$), data between two end states are intentionally ignored. Because of dismissing $V_{\beta'}$ value, we need to produce another equation in substitution. Consequently, the next task is to obtain a relationship between $T_{j\alpha}$ and $T_{j\beta'}$ based on the principle of thermal anchoring. Following the first law of thermodynamics, we identify all energy components crossing the boundary of the sample's control volume (Fig. 1a), and write $P_{elec} = P_{opt}(t) + P_{conv}(t) + P_{rad}(t) + P_{cond}(t)$ (Supplementary S4). Finally, from state β' to state γ, we are allowed to utilize the steady-state V & T_j relationship, which is approximately linear with a negative slope. If time between β and β' is taken to be 100 ms, we obtain $T_{j\alpha} = 75.0\,^\circ$C for B1# sample (Supplementary S5). Since it remains uncertain to precisely locate the state β', next we propose a previously-unreported method that adopts the principle of thermal anchoring and avoids PISO. In the steady-state Shockley equation for diodes, namely,

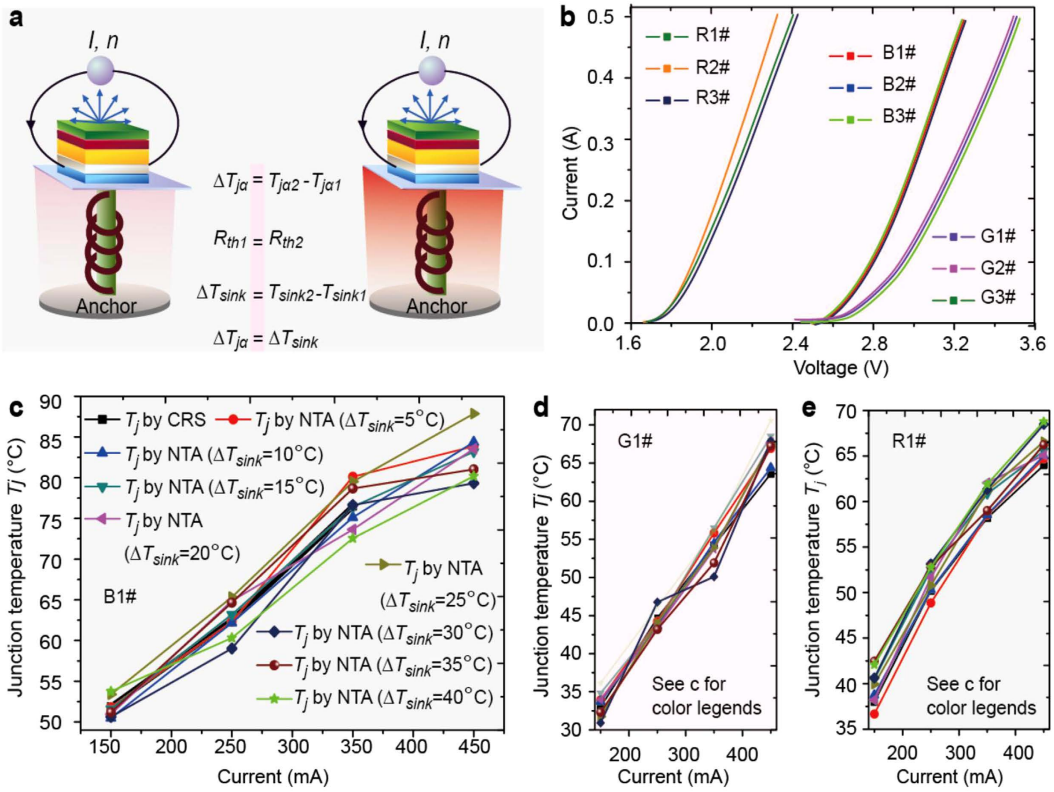

Figure 4. Schematic of nonlinear thermal-anchoring (NTA) and T_j results. (**a**) In thermal anchoring, T_{sink} behaves as the anchor, which is maintained constant by the temperature controller, and can also transport the thermal energy away to outside the sample. The experimental procedure includes: (1) set $T_{sink1} = 25.0$ °C, and obtain I-V characteristic curves of nine LED samples for various currents ranging from 1 mA to 500 mA. Measurements are taken 300 s after the current is switched on, assuring that the steady state was reached. (2) set $T_{sink2} = 35.0$ °C and measure I-V characteristic curves as step (1). (**b**) IV characteristic curves measured according to the experimental procedure in **a** for nine samples at $T_{sink} = 25.0$ °C. These curves for same-colored samples appear almost indistinguishable. (**c**) T_j measured using NTA for B1# sample. (**d**) T_j measured using NTA for G1# sample. (e) T j measured using NTA for R1# sample. NTA for G1# sample. (**e**) T_j measured using NTA for R1# sample.

$$I = I_s\left[exp\left(\frac{qV}{nkT}\right) - 1\right]. \tag{3}$$

Since I, I_s and V can be readily measured via experiments, we have only the ideality factor n and T_j left as unknowns, and need one more equation.

In analogy to casting the anchor when docking a ship in the harbor so that the anchor location reveals ships' whereabouts, we maintain T_{sink} constant and attempt to determine T_j. The overall thermal resistance of two layers, namely the die attach, and Cu slug, between the LED chip and the sink resembles the length of the anchoring steel wire.

In reference to the physical configuration of the sample (Fig. 1a), it is reasonable to idealize these layers as one-dimensional slabs. Consider a multi-layer system whose top and bottom are either heat sinks or sources. We further recognize the phenomenon that, when phonon waves propagate from the source to the sink, they excite oscillations of lattice inertia along the path, but do not alter basic lattice structures after they pass. When they reach the sink, T_{sink} remains constant, but vibration energy escapes to outside the sink, and thermal conductivities of intermediate layers remain unchanged. If the electrical input P_{elec} also remains unchanged (implying P_{cond} remains the same), so does $T_j - T_{sink}$. Then, we select two states, 1 and 2, where 1 represents $T_{sink1} = 25.0$ °C; 2 denotes $T_{sink2} = 35.0$ °C (10.0 degrees higher than T_{sink1}. Other T_{sink} differences ranging from 5.0 °C to 40.0 °C with a 5.0 °C increment have also been conducted). Under the iso-current condition ($I = 350$ mA), we observe that P_{th1} equals P_{th2} (because V varies minimally) and that $R_{th1} = R_{th2}$ (for example, k_{Cu} varies from 413.0 to 393.0 W/mK when its temperature varies from 200 K to 400 K)[32]. Therefore, we can safely deduce $T_{j\alpha 1} - T_{sink1} \approx T_{j\alpha 2} - T_{sink2}$ (Fig. 4a,b). As a result, we obtain two nonlinear relations,

$$I = I_s(T_{j\alpha 1})exp\left(\frac{qV_1}{nkT_{j\alpha 1}}\right), \tag{4}$$

and

$$I = I_s\left(T_{j\alpha 1} + \Delta T_{\text{sink}}\right)exp\left(\frac{qV_2}{nk\left(T_{j\alpha 1} + \Delta T_{\text{sink}}\right)}\right), \tag{5}$$

where $\Delta T_{sink1} = T_{sink2} - T_{sink1}$. Equations (4) and (5) can be simultaneously solved using the Newton-Raphson method[33] or its modified version (Supplementary S6). Values of T_j agree well with those obtained using CRS, TC and TI (Fig. 4c–e). Additionally, we have found this T_{sink} difference of 10.0 °C to be optimal among other T_{sink} differences. If T_{sink} becomes too large, R_{th} no longer remains constant, violating the nonlinear thermal anchoring principle. If T_{sink} becomes too small, two algebraic equations tend to be similar, leading to algebraic redundancy.

Steps of the procedure can be outlined as:

(a) Measure the reverse current versus the junction temperature to obtain $I_s\left(T_j\right)$.
(b) Measure the $I - V$ characteristic curve from 1 mA to 500 mA at $T_{sink1} = 25.0$ °C and $T_{sink2} = 35.0$ °C, respectively
(c) To solve equations (4) and (5) using Newton-Raphson method to obtain $T_{j\alpha 1}$ at $T_{sink1} = 25.0$ °C.

In summary, the discrepancy between PISO and non-PISO is attributed to non-synchronization of lattice and carrier temperatures in transient states. Generally in PISO carrier transient behaviors are intentionally bypassed, rendering the voltage and the carrier's temperature disengaged. To confirm and avoid this PISO-induced disengagement, we first discover the LITA mechanism and develop an original, accurate, and nondestructive technique to measure LED junction temperatures in steady state conditions. This principle of the nondestructive method involves $I - V$ characteristic of LEDs and nonlinear thermal anchoring. Finally, NTA results exhibit close agreements with data of Raman spectroscopy, thermal couples, and thermal imagers (Fig. 4c–e, Fig. S3a,b).

Methods

Forward voltage method. FVM includes three primary steps: (a) obtain a steady-state linear relationship between the voltage and T_j (inset of Fig. 2a), (b) operate PISO from state α to state β, and (c) allow the sample to cool down from state β to state γ (steady state) (Fig. 2a). Take blue InGaN/GaN LED (B1#) as the example. At three sink temperatures (25.0 °C, 35.0 °C, and 45.0 °C) and $I_\beta = 5$ mA, we measure three different voltages (2.565 V, 2.555 V, and 2.543 V), and obtain a negative-sloped line representing the relationship between V and T_j, with $k_V = -1.2$ mV/K (inset). Next, we run a steady state current at $I_\alpha = 350$ mA for 5 minutes. Instantaneously, the current is switched down to $I_\beta = 5$ mA with the duration lasting approximately 1 μs. At this instant, the voltage, V_β, is recorded. After approximately 5 more minutes, the voltage is recorded to be V_γ. In reference to the linear relationship between V and T_j, we deduce the value of $T_{j\beta}$, according to $V_\beta - V_\gamma = k_V\left(T_{j\beta} - T_{j\gamma}\right)$, to be 36.8 °C, which is assumed to equal $T_{j\alpha}$ in FVM.

Confocal Raman spectroscopy. CRS includes two primary steps: (a) measure Raman shifts for various $T_j = T_{sink}$ values to obtain a relationship between Raman shift and T_j when LED is lit at small currents (5 mA). The LED sample is mounted on a heat sink, controlled by a temperature controller (Keithley Instruments, Inc., American, Keithley 2510), and is lit by a current source (Keithley Instruments, Inc., American, Keithley 2611). (b) measure Raman shifts to obtain desired T_j when LED is litby large currents. Raman shift signals are collected by a confocal Raman microscope (XploRA, HORIBA Jobin Yvon, France) to yield a correlation between the wave-peak location and the junction temperature when the LED is lit at small currents (5 mA). After the acquisition of this shift and T_j relationship, we turn on the LED at large currents and measure the Stokes shift again. Because the B1 chip emits 400 ~ 550 nm light beams, we select the 633 nm laser, carefully maintain all parametric conditions the same as the small-current run at $T_{sink} = 25.0$ °C, and measure Raman shifts under currents of 150 mA, 250 mA, and 350 mA.

Thermocouples. TCs are placed on the sample surface for several random positions and take average values (Supplementary S1).

Thermal imager. TI aims at the chips surface and takes the average of measurements distributed within a pre-determined area (Supplementary Fig. S1b–d).

Nonlinear thermal-anchoring. NTA principle combined with Shockley equation generates two nonlinear equations which are solved by Newton-Raphson method. All first-order derivatives are discretized using the finite difference method, with the occasional necessary to adopt the under-relaxation algorithm to achieve convergences.

References

1. Nakamura, S., Amano, H. & Akasaki, I. For the invention of efficient blue light-emitting diodes which has enabled bright and energy-saving white light sources. Nobel Prize in Physics (2014) Available at: http://www.nobelprize.org /nobel_prizes/physics/laureates/2014/. (Accessed: 4th December 2015)
2. Schubert, E. F. & Kim, J. K. Solid-state light sources getting smart. *Science* **308,** 1274–1278 (2005).
3. Ponce, F. A. & Bour, D. P. Nitride-based semiconductors for blue and green light-emitting devices. *Nature* **386,** 351–359 (1997).
4. Ng, W. L. *et al.* An efficient room-temperature silicon-based light-emitting diode. *Nature* **410,** 192–194 (2001).
5. Jennifer, A. L. & Bok, Y. A. Three-dimensional printed electronics. *Nature* **518,** 42–43 (2015).
6. Nam, H. *et al.* Improved heat dissipation in gallium nitride light-emitting diodes with embedded grapheme oxide pattern. *Nat. Comm*. **4,** 1452–1460 (2013).
7. Lukyanchuk, B. *et al.* The Fano resonance in plasmonic nanostructures and metamaterials. *Nature Mater*. **9,** 707–715 (2010).
8. Yan, W. & Zhi, X. The critical power to maintain thermally stable molecular junctions. *Nat. Comm*. **5,** 4297–4303 (2014).
9. Khan, A., Balakrishnan, K. & Katona, T. Ultraviolet light-emitting diodes based on group three nitrides. *Nature Photon*. **2,** 77–84 (2008).
10. Saniya, D., Junseok, H., Ayan, D. & Pallab, B. Electrically driven polarized single-photon emission from an InGaN quantum dot in a GaN nanowire. *Nat. Comm*. **4,** 1675–1683 (2013).
11. Wierer, J. J., David, A. & Megens, M. M. III-nitride photonic-crystal light-emitting diodes with high extraction efficiency. *Nature Photon*. **3,** 163–169 (2009).
12. Schleeh, J. Phonon black-body radiation limit for heat dissipation in electronics. *Nature Mater*. **14,** 187–192 (2015).
13. Zheludev, N. The life and times of the LED a 100-yearhistory. *Nature Photon*. **1,** 189–192 (2007).
14. Vogl, U. & Weitz, M. Laser cooling by collisional redistribution of radiation. *Nature* **461,** 70–73 (2009).
15. Shun, W. *et al.* Polaron spin current transport in organic semiconductors. *Nature Photon*. **10,** 308–313 (2014).
16. Xi, Y. & Schubert, E. F. Junction-temperature measurement in GaN ultraviolet light-emitting diodes using diode forward voltage method. *Appl. Phys. Lett*. **85,** 2163–2165 (2004).
17. Xi, Y. *et al.* Junction and carrier temperature measurements in deep-ultraviolet light emitting diodes using three different methods. *Appl. Phys. Lett*. **86,** 031907 (2005).
18. Hall, D. C., Goldberg, L. & Mehuys, D. Technique for lateral temperature profiling in optoelectronic devices using a photoluminescence microprobe. *Appl. Phys. Lett*. **61,** 384 (1992).
19. Rommel, J. M., Gavrilovic, P. & Dabkowski, F. P. Photoluminescence measurement of the facet temperature of 1W gain-guided AlGaAs/GaAs laser diodes. *J. Appl. Phys*. **80,** 6547 (1996).
20. Wu, B. Q. *et al.* Junction-temperature determination in InGaN light-emitting diodes using reverse current method. *IEEE Trans. Electron Devices* **60,** 241–245 (2013).
21. Lin, S. Q. *et al.* Determining junction temperature in InGaN light-emitting diodes using low forward currents. *IEEE Trans. Electron Devices* **60,** 3775–3779 (2013).
22. Wang, Y. *et al.* Temperature measurement of GaN-based ultraviolet light-emitting diodes by micro-Raman spectroscopy. *J. Electron. Mater*. **39,** 2448–2451 (2010).
23. Ren, B. *et al.* Optimizing detection sensitivity on surface-enhanced Raman scattering of transition-metal electrodes with confocal Raman microscopy. *Appl. Spectrosc*. **57,** 419–427 (2003).
24. Wang, X. *et al.* Probing the location of hot spots by surface-enhanced Raman spectroscopy: toward uniform substrates. *ACS Nano*. **8,** 528–536 (2014).
25. Fu, X. & Luo, X. B. Can thermocouple measure surface temperature of light emitting diode module accurately? *Int. J. Heat Mass Transfer* **65,** 199–202 (2013).
26. Zhang, J. H. *et al.* Thermal analyses of alternating current light-emitting diodes. *Appl. Phys. Lett*. **103,** 153505 (2013).
27. Markus, B., Claus, R. & Thomas, E. Ultrafast carrier dynamics in graphite. *Phys. Rev. Lett*. **102,** 086809 (2009).
28. Van, V. J. A. & Wautelet, M. Variation of semiconductor band gaps with lattice temperature and with carrier temperature when these are not equal. *Phys. Rev. B* **23,** 5543–5550 (1981).
29. Lietoila, A. & Gibbons, J. F. Calculation of carrier and lattice temperatures induced in Si by picosecond laser pulses. *Appl. Phys. Lett*. **40,** 624–626 (1982).
30. Sun, C. K., Choi, H. K., Wang, C. A. & Fujimoto, J.G. Studies of carrier heating in InGaAs/AlGaAs strained-layer quantum well diode lasers using a multiple wavelength pump probe technique. *Appl. Phys. Lett*. **62,** 747–749 (1993).
31. Knox, W. H. *et al.* Femtosecond excitation of nonthermal carrier populations in GaAs quantum wells. *Phys. Rev.Lett*. **56,** 1191–1193 (1986).
32. Bergman, T. L., Lavine, A. S., Incropera, F. P. & Dewitt, D. P. *Fundamentals of Heat and Mass Transfer Ch. 2* (John Wiley & Sons, Inc., Hoboken, 2011).
33. Fujiwara, K., Nakata, T., Okamoto, N. & Muramatsu, K. Method for determining relaxation factor for modified Newton-Raphson method. *IEEE Trans. Magn*. **29,** 1962–1965 (1993).

Acknowledgements

This work was supported in part by the 863 project of China under Grant 2013 AA03A107, Major Science and Technology Project between University-Industry Cooperation in Fujian Province under Grant No. 2013 H6024, Shineraytek Optoelectronics Co., LED Cooling Project 2013−2016, and the Institute for Complex Adaptive Matter, University of California, Davis under Grant ICAM-UCD13−08291.

Author Contributions

J.H.Z. and T.M.S. conceived the original concept, performed experiments, and wrote the manuscript. Y.J.L., H.M. and Z.C. participated in technical planning and discussions. R.R.C. and Z.C. provided useful consultations.

Additional Information

Supplementary information accompanies this paper at http://www.nature.com/srep

Competing financial interests: The authors declare no competing financial interests.

How to cite this article: Zhang, J. *et al.* Non-synchronization of lattice and carrier temperatures in light-emitting diodes. *Sci. Rep.* **6**, 19539; doi: 10.1038/srep19539 (2016).